Subharmonic and Combination Resonance of Rotating Pre-deformed Blades Subjected to High Gas Pressure

Bo Zhang[1,2]   **Hu Ding**[3]   **Li-Qun Chen**[3⋆]

([1]*School of Science, Chang'an University, Xi'an 710064, Shaanxi, China*)
([2]*Shanghai Institute of Applied Mathematics and Mechanics, Shanghai University, Shanghai 200444, China*)
([3]*School of Science, Harbin Institute of Technology, Shenzhen 518055, China*)

ABSTRACT The present paper deals with the investigation of dynamic responses of a rotating pre-deformed blade in four cases of resonance, including two subharmonic resonances and two combination resonances. The dimensionless gas excitation amplitude is assumed to share the same order with the dimensionless vibration displacement. Four cases of resonance are confirmed by examining the secular terms. The theoretical analysis framework is established for each resonance case based on the method of multiple scales. The original dynamic system is integrated numerically by the Runge–Kutta method. The frequency components and phases obtained from fast Fourier transform of the numerical response are used to verify the theoretical results. For the purpose of contrast, modulation equations are also integrated numerically. In all four resonance cases, the theoretical results agree well with the numerical simulation. Parameter studies are conducted to clarify the effects of system parameters on the perturbation curves. Various results are obtained for the rotating blade. A quasi-saturation phenomenon occurs in both combination resonances of summed type and difference type, and the corresponding limit value of the second-mode response can be reduced by decreasing the external detuning parameter. The quasi-saturation phenomenon of rotating blade only appears with high gas pressure. The subharmonic resonance of second mode and the combination resonance of summed type are hard to excite in practice compared with the other two cases.

KEY WORDS Internal resonance, Subharmonic resonance, Combination resonance, Rotating blade, Stability

1. Introduction

Rotating blades are present in many industry applications. The aircraft engine is one of the most important instances. Blade vibration failure due to resonance and flutter occupies a large proportion of the total engine failure. A better understanding of the resonance mechanism and dynamic behavior of rotating blades is helpful to reduce blade vibration failure.

In the early studies [1–6] of this field, researchers presented numerous dynamic modeling methodologies of rotating blades and investigated the dynamic characteristics of such structures with only some classical effects taken into consideration in the framework of small-deformation theory. Afterwards, some researchers also paid their attention to some nonclassical effects on the dynamic characteristics

---

⋆ Corresponding author. E-mail: chenliqun@hit.edu.cn

of rotating blade. Qin et al. [7] addressed the influence of hygrothermal environment on a rotating composite blade. Liang et al. [8] clarified the contributions of gyroscopic term and dynamic centrifugal terms on a rotating blade. Niu et al. [9] built a dynamic model for a rotating functionally graded cylindrical panel reinforced with graphene platelets (GPLs). Zhang et al. [10] examined the natural frequencies of the rotating blade with different distribution patterns, weight fractions and geometric characteristics of the GPLs. Guo et al. [11] studied the coupling effects among six displacement components based on the Timoshenko beam theory. Xie et al. [12] modeled a rotating blade with a breathing crack.

In reality, the engine blade often serves under the extreme environment. The flow field around the rotating blades is highly unsteady and turbulent. The large amplitude vibration is unavoidable under strong periodic gas flow disturbance [13]. Results and conclusions obtained based on the small-deformation theory seem to be inadequate. Hence, an increasing number of researchers have been focusing their attention on the nonlinear dynamic behavior of such structures nowadays, especially on the internal resonance behavior due to its potential threat to the fatigue life of rotating blades [14]. Li et al. [15] modeled a wind turbine blade considering the geometric nonlinearities and studied the effects of aerodynamic loads on the dynamic characteristics of the blade. Recently, Yao et al. [16] established a dynamic model of a pre-twisted blade based on the shell theory and reported the influences of system parameters on the nonlinear dynamic response of the blade. Thomas et al. [17] studied the nonlinear vibration of a rotating blade considering the large deformation. They reported that rotating speed could affect the hardening/softening behavior and the jumping phenomena. Wang et al. [18] studied the 1:1 internal resonance of a turbine blade considering the fluid-structure interactions. Zhang et al. [19] established a nonlinear dynamic model of rotating pre-twisted blade considering the pre-deformation caused by the thermal gradient. They verified the possibility of the occurrence of 2:1 internal resonance and conducted parameter studies to reveal the nonlinear dynamic behavior of the blade. Zhang et al. [20] explored the second primary resonance of the same blade and presented a saturation phenomenon.

In the above studies, researchers studied the dynamic behavior of rotating blades when primary resonance occurs, that is, the exciting frequency is near one of the natural frequencies of the blade. There exist more complex resonance mechanisms in the nonlinear system. Other exciting frequencies could also result in resonance, such as super-harmonic resonance, subharmonic resonance and combination resonance. Cao et al. [21] constituted the Campbell diagram of a pre-twisted rotating plate to demonstrate the possibility of complex harmonic resonances in such structures when nonlinearities are taken into account. Inoue et al. [22] validated the occurrence of super-harmonic resonance of a wind turbine blade in their experiment. Recently, Zhang et al. [23] studied the super-harmonic resonance of a rotating blade based on the previous dynamic model [19]. Shahgholi et al. [24] utilized the harmonic balance method to address the combination and subharmonic resonances of a rotating shaft. From the literature review, it could be concluded that although the subharmonic resonance [25] and combination resonance [26, 27] have been studied for various structures, the related theoretical analyses of the dynamic responses of pre-deformed rotating blades, especially those subjected to high gas pressure, are rather limited. To close the gap, we consider four cases of resonances, including two subharmonic resonances and two combination resonances, and calculate the corresponding steady-state response of a rotating blade in this study.

2. Equations of Motion and Analytical Solutions

Consider a rotating pre-twisted blade attached to a disk with a certain setting angle, as shown in Fig. 1. The rotating speed of the disk is Ω. A strong harmonic gas pressure P_{gas} is acted on the blade. The blade serves in a thermal gradient environment. The notations g_y and g_z denote the thermal gradients in two principle directions, i.e., the width direction and the thickness direction of the blade section, respectively. It must be mentioned that the present load status of the blade is rather idealized, and is a simplification of the real one. In reality, the turbine blade suffers from complex loads, for example, the blade-casing impact and rubbing, the air blast loads, etc. The detailed consideration of the complex loads exerted on the turbine blade exceeds the scope of the present investigation, which, however, is a challenging and rewarding research direction. For details of the force state on blades, readers are referred to [16, 28, 29].
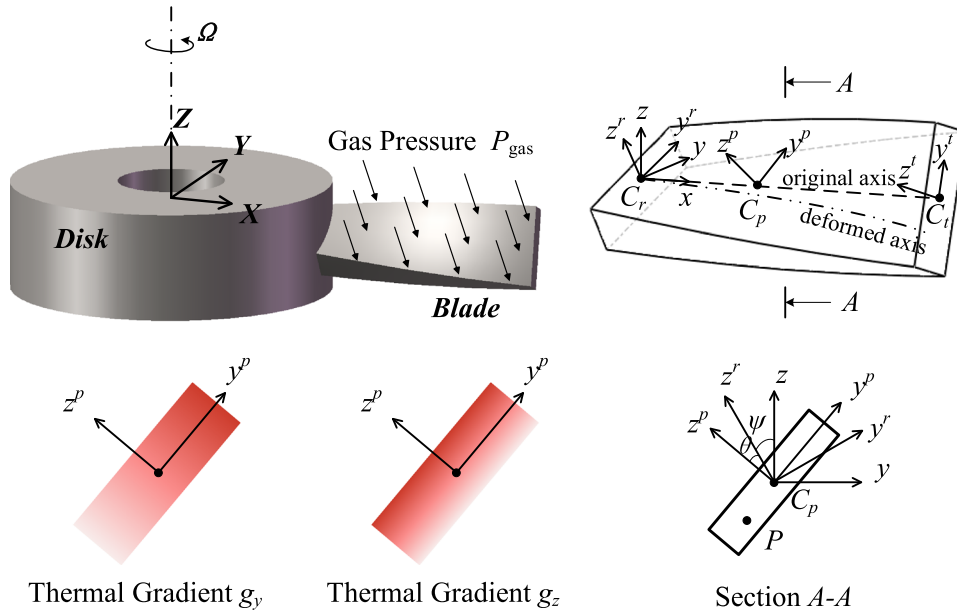
Fig. 1. The model of a rotating pre-deformed blade subjected to gas pressure

The governing equation of the blade, including the effects of geometric large deformation and the pre-deformation caused by thermal gradient, could be derived via Lagrange principle and modal transformation [20].

$$\ddot{\tilde{q}}_i + c_d \dot{\tilde{q}}_i + \omega_i^2 \tilde{q}_i = \tilde{f}_i \cos(\omega t) + \sum_{j=1}^{n_2+n_3} \sum_{k=1}^{n_2+n_3} \eta_{ijk} \tilde{q}_j \tilde{q}_k + \sum_{j=1}^{n_2+n_3} \sum_{k=1}^{n_2+n_3} \sum_{l=1}^{n_2+n_3} \xi_{ijkl} \tilde{q}_j \tilde{q}_k \tilde{q}_l \quad (i=1,2\ldots,n_2+n_3)$$

(1)

in which, $\tilde{q}_i$ and $\tilde{f}_i$ denote the system response and the excitation amplitude in modal space, respectively. Here, $\tilde{f}_i$ are proportional to the gas pressure amplitude P_{gas}. The symbols c_d and ω_i are the dimensionless damping coefficient and the blade dimensionless natural frequencies, respectively. η_{ijk} are the quadratic nonlinear coefficients introduced by the pre-deformation. ξ_{ijkl} are the cubic nonlinear coefficients introduced by the large deformation, which is proved to be ignorable, especially in the presence of 2:1 internal resonance in the previous study [20]. n_2 and n_3 are the numbers of trial functions assumed chordwise and flapwise, respectively.

The previous studies [19, 20] were confined to the resonance mechanism and dynamic behavior of rotating blade under weak excitation. In the present study, a strong gas pressure is applied to the blade. Hence, the excitation amplitude is assumed to have the same order as the blade response [30]. The vibration response, damping coefficient and gas pressure are rescaled as follows.

$$\tilde{q}_i \leftrightarrow \varepsilon \tilde{q}_i, c_d \leftrightarrow \varepsilon c_d, \tilde{f}_i \leftrightarrow \varepsilon \tilde{f}_i$$

(2)

where ε is a small dimensionless parameter. The solution of the system is assumed to have the following form

$$\tilde{q}_i(t) = \tilde{q}_{i0}(T_0, T_1) + \varepsilon \tilde{q}_{i1}(T_0, T_1) + O(\varepsilon^2)$$

(3)

in which $T_0 = t$ and $T_1 = \varepsilon t$ are the fast and slow time scales, respectively. Then we substitute Eqs. (2) and (3) into Eq.(1) and set the coefficients of each power of ε to be zero. The following equations can be obtained.

$$D_0^2 \tilde{q}_{i0} + \omega_i^2 \tilde{q}_{i0} = \tilde{f}_i \cos(\omega T_0)$$

(4)

$$D_0^2 \tilde{q}_{i1} + \omega_i^2 \tilde{q}_{i1} = -2D_0 D_1 \tilde{q}_{i0} - c_d D_0 \tilde{q}_{i0} + \sum_{j=1}^{n_2+n_3} \sum_{k=1}^{n_2+n_3} \eta_{ijk} \tilde{q}_{j0} \tilde{q}_{k0}$$

(5)

where D_i $(i = 0, 1)$ represents the derivative operator $\partial/\partial T_i$. It should be noted that the derivative operator will also get perturbed after the multiple time scales are introduced. The solution to Eq. (4) holds the following form.

$$\tilde{q}_{i0} = A_i (T_1) \exp (i\omega_i T_0) + B_i \exp (i\omega T_0) + \text{cc} \tag{6}$$

which consists of the general solution (i.e. the free vibration component) and the particular solution (i.e. the forced vibration component). A_i and B_i denote the corresponding amplitudes. The symbol cc denotes the complex conjugate of the terms ahead. A_i and B_i can be written as:

$$A_i (T_1) = \frac{a_i (T_1)}{2} \exp (i\zeta_i (T_1)) , B_i = \frac{\tilde{f}_i}{2 (\omega_i^2 - \omega^2)} \tag{7}$$

$A_i(T_1)$ is an undetermined complex function of T_1, while B_i is a real. a_i and ζ_i stand for the magnitude and phase angle of $A_i(T_1)$, respectively. Substituting Eq. (6) into Eq. (5) yields

$$
\begin{aligned}
D_0^2 \tilde{q}_{i1} + \omega_i^2 \tilde{q}_{i1} = &-i\omega_i (2D_1 A_i + c_d A_i) \exp (i\omega_i T_0) - i\omega c_d B_i \exp (i\omega T_0) \\
&+ \sum_{j=1}^{n_2+n_3} \sum_{k=1}^{n_2+n_3} \eta_{ijk} \{ B_j B_k \exp (2i\omega T_0) \\
&+ A_j A_k \exp (i (\omega_j + \omega_k) T_0) + A_j \bar{A}_k \exp (i (\omega_j - \omega_k) T_0) + A_j B_k \exp (i (\omega_j + \omega) T_0) \\
&+ \bar{A}_j B_k \exp (i (\omega - \omega_j) T_0) + B_j A_k \exp (i (\omega_k + \omega) T_0) + B_j \bar{A}_k \exp (i (\omega - \omega_k) T_0) \} + \text{cc}
\end{aligned}
\tag{8}
$$

The possibility of the 2:1 internal resonance, i.e. $2\omega_1 \approx \omega_2$, has been confirmed in the present model [19]. The internal detuning parameter σ_1 is introduced to describe the nearness between ω_2 and $2\omega_1$, $\omega_2 = 2\omega_1 + \varepsilon\sigma_1$. Hence, the term $A_j \bar{A}_k \exp (i (\omega_j - \omega_k) T_0)$ $(j = 2, k = 1)$ and the term $A_j A_k \exp (i (\omega_j + \omega_k) T_0)$ $(j = k = 1)$ will contribute to the secular terms for the first and the second modes, respectively. In the present study, our attention is focused on the cross terms, such as the term $A_j B_k \exp (i (\omega_j + \omega) T_0)$ and the term $\bar{A}_j B_k \exp (i (\omega - \omega_j) T_0)$. When the excitation frequency ω is set as several special values, the cross terms can also contribute to the secular terms.

2.1. The Case of ω Being Close to $2\omega_1$

When ω is close to $2\omega_1$, the term $\bar{A}_j B_k \exp (i (\omega - \omega_j) T_0)$ $(j = 1, k = 1$ or $2)$ contributes to the secular terms of the first mode. In addition, the term $-i\omega c_d B_i \exp (i\omega T_0)$ $(i = 1)$ can also contribute to the secular terms of the second mode due to the presence of the 2:1 internal resonance. In the present case, B_2 is a small divisor term. This resonance is often defined as the subharmonic resonance of the first mode. The external detuning parameter σ_2 is introduced as $\omega = 2\omega_1 + \varepsilon\sigma_2$. Eliminating the secular terms of the first two modes yields the solvability conditions.

$$
\begin{aligned}
D_1 A_1 &= \Gamma_{11} A_1 + \Gamma_{12} \bar{A}_1 A_2 \exp(i\sigma_1 T_1) + \Gamma_{13} \bar{A}_1 \exp (i\sigma_2 T_1) \\
D_1 A_2 &= \Gamma_{21} A_2 + \Gamma_{22} A_1^2 \exp(-i\sigma_1 T_1) + \Gamma_{23} \exp(i (\sigma_2 - \sigma_1) T_1)
\end{aligned}
\tag{9}
$$

where

$$\Gamma_{11} = \Gamma_{21} = -c_d/2, \Gamma_{12} = (\eta_{121} + \eta_{112})/(2i\omega_1), \Gamma_{22} = \eta_{211}/(2i\omega_2), \Gamma_{13} = B_1 \sum_{k=1}^{n_2+n_3} (\eta_{11k} + \eta_{1k1})/2i\omega_1,$$

$$\Gamma_{23} = -\omega c_d B_2/2\omega_2 \tag{10}$$

Separating the real from the imaginary part on both sides of Eq. (9), one can derive the autonomous modulation equations.

$$\frac{\mathrm{d}a_1}{\mathrm{d}T_1} = \left(\Gamma_{12}^R \cos \psi_1 - \Gamma_{12}^I \sin \psi_1\right) \frac{a_1 a_2}{2} + \left(\Gamma_{13}^R \cos \psi_2 - \Gamma_{13}^I \sin \psi_2\right) a_1 + \Gamma_{11}^R a_1$$

$$\frac{\mathrm{d}a_2}{\mathrm{d}T_1} = 2\left[\Gamma_{23}^R \cos(\psi_2 - \psi_1) - \Gamma_{23}^I \sin(\psi_2 - \psi_1)\right] + \Gamma_{21}^R a_2 + \left(\Gamma_{22}^R \cos \psi_1 + \Gamma_{22}^I \sin \psi_1\right) \frac{a_1^2}{2}$$

$$\frac{\mathrm{d}\psi_1}{\mathrm{d}T_1} = \left[\Gamma_{23}^R \sin(\psi_2 - \psi_1) + \Gamma_{23}^I \cos(\psi_2 - \psi_1)\right] \frac{2}{a_2} - \left(\Gamma_{22}^R \sin \psi_1 - \Gamma_{22}^I \cos \psi_1\right) \frac{a_1^2}{2a_2} - \left(\Gamma_{12}^R \sin \psi_1\right. \tag{11}$$

$$\left. + \Gamma_{12}^I \cos \psi_1\right) a_2 - 2\left(\Gamma_{13}^R \sin \psi_2 + \Gamma_{13}^I \cos \psi_2\right) + \sigma_1 + \Gamma_{21}^I - 2\Gamma_{11}^I$$

$$\frac{\mathrm{d}\psi_2}{\mathrm{d}T_1} = -\left(\Gamma_{12}^R \sin \psi_1 + \Gamma_{12}^I \cos \psi_1\right) a_2 - 2\left(\Gamma_{13}^R \sin \psi_2 + \Gamma_{13}^I \cos \psi_2\right) + \sigma_2 - 2\Gamma_{11}^I$$

where $\psi_1 = \sigma_1 T_1 - 2\zeta_1 + \zeta_2$, $\psi_2 = \sigma_2 T_1 - 2\zeta_1$, and the real part and imaginary part of coefficients Γ_{ij} are denoted by superscripts R and I, respectively. Given that the left side of Eq. (11) is equal to 0 in the steady state, the modulation equations lead to a set of nonlinear quaternary algebraic equations. Apparently, the solutions of the algebraic equations include two types: the single-mode solution ($a_1 = 0$ and $a_2 \neq 0$), and the coupled-mode solution ($a_1 \neq 0$ and $a_2 \neq 0$). Substituting $a_1 = 0$ into the right side of Eq. (11), one can obtain the single-mode solution as follows.

$$a_{1l} = 0, \ a_{2l} = 2|\Gamma_{23}|/\sqrt{\left(\Gamma_{21}^R\right)^2 + \left(\sigma_2 - \sigma_1 - \Gamma_{21}^I\right)^2} \tag{12}$$

In the present case, it is hard to derive the analytical expressions of the coupled-mode solution. The command "NSolve" in Mathematica is employed to find numerical approximations of the corresponding equations.

In order to determine the stability of these two types of solution, it is convenient to cast the modulation equations into the Cartesian form as follows.

$$\frac{\mathrm{d}x_1}{\mathrm{d}T_1} = \left(\Gamma_{11}^R + \Gamma_{13}^R\right) x_1 + \left(\Gamma_{11}^I - \Gamma_{13}^I\right) y_1 - \nu_1 y_1 + \frac{1}{2}\Gamma_{12}^R \left(x_1 x_2 + y_1 y_2\right) + \frac{1}{2}\Gamma_{12}^I \left(x_1 y_2 - x_2 y_1\right)$$

$$\frac{\mathrm{d}y_1}{\mathrm{d}T_1} = -\left(\Gamma_{11}^I + \Gamma_{13}^I\right) x_1 + \left(\Gamma_{11}^R - \Gamma_{13}^R\right) y_1 + \nu_1 x_1 - \frac{1}{2}\Gamma_{12}^I \left(x_1 x_2 + y_1 y_2\right) + \frac{1}{2}\Gamma_{12}^R \left(x_1 y_2 - x_2 y_1\right)$$

$$\frac{\mathrm{d}x_2}{\mathrm{d}T_1} = \Gamma_{21}^R x_2 + \Gamma_{21}^I y_2 - \nu_2 y_2 + \frac{1}{2}\Gamma_{22}^R \left(x_1^2 - y_1^2\right) + \Gamma_{22}^I x_1 y_1 + 2\Gamma_{22}^R \tag{13}$$

$$\frac{\mathrm{d}y_2}{\mathrm{d}T_1} = -\Gamma_{21}^I x_2 + \Gamma_{21}^R y_2 + \nu_2 x_2 - \frac{1}{2}\Gamma_{22}^I \left(x_1^2 - y_1^2\right) + \Gamma_{22}^R x_1 y_1 - 2\Gamma_{22}^I$$

in which $\nu_1 = \sigma_2/2$, $\nu_2 = \sigma_2 - -\sigma_1$. The eigenvalues of the Jacobian matrix of Eq. (13) are calculated at the steady-state solutions. If there exist positive real parts among the eigenvalues, the corresponding solution is unstable.

Ultimately, the first approximate solutions can be written as

$$\tilde{q}_1 = a_1 \cos\left(\omega t/2 - \psi_2/2\right) + 2B_1 \cos\left(\omega t\right) + O\left(\varepsilon^2\right)$$

$$\tilde{q}_2 = a_2 \cos\left(\omega t + (\psi_1 - \psi_2)\right) + 2B_2 \cos\left(\omega t\right) + O\left(\varepsilon^2\right) \tag{14}$$

$$\tilde{q}_i = 0 \quad (i = 3, 4, \cdots, n_2 + n_3)$$

2.2. The Case of ω Being Close to $2\omega_2$

When ω is close to $2\omega_2$, the term $\bar{A}_j B_k \exp\left(\mathrm{i}\left(\omega - \omega_j\right) T_0\right)$ ($j = 2$, $k = 1$ or 2) contributes to the secular terms of the second mode. This resonance is often defined as the subharmonic resonance of the second mode. The external detuning parameter σ_2 is introduced as $\omega = 2\omega_2 + \varepsilon\sigma_2$. After the mathematic

manipulations similar to those in subsection 2.1, we can obtain the polar form of modulation equations

$$\frac{da_1}{dT_1} = \Gamma_{11}^R a_1 + \left(\Gamma_{12}^R \cos\psi_1 - \Gamma_{12}^I \sin\psi_1\right)\frac{a_1 a_2}{2}$$

$$\frac{da_2}{dT_1} = \Gamma_{21}^R a_2 + \left(\Gamma_{22}^R \cos\psi_1 + \Gamma_{22}^I \sin\psi_1\right)\frac{a_1^2}{2} + \left(\Gamma_{24}^R \cos\psi_2 - \Gamma_{24}^I \sin\psi_2\right) a_2$$

$$\frac{d\psi_1}{dT_1} = \sigma_1 + \Gamma_{21}^I - \left(\Gamma_{22}^R \sin\psi_1 - \Gamma_{22}^I \cos\psi_1\right)\frac{a_1^2}{2a_2} + \left(\Gamma_{24}^R \sin\psi_2 + \Gamma_{24}^I \cos\psi_2\right) - 2\Gamma_{11}^I$$
$$\qquad - \left(\Gamma_{12}^R \sin\psi_1 + \Gamma_{12}^I \cos\psi_1\right) a_2$$

$$\frac{d\psi_2}{dT_1} = \sigma_2 - 2\Gamma_{21}^I + \left(\Gamma_{22}^R \sin\psi_1 - \Gamma_{22}^I \cos\psi_1\right)\frac{a_1^2}{a_2} - 2\left(\Gamma_{24}^R \sin\psi_2 + \Gamma_{24}^I \cos\psi_2\right) \tag{15}$$

where

$$\psi_1 = \sigma_1 T_1 - 2\zeta_1 + \zeta_2,\ \psi_2 = \sigma_2 T_1 - 2\zeta_2,\ \Gamma_{24} = \sum_{k=1}^{n_2+n_3}(\eta_{22k} + \eta_{2k2})B_k/2i\omega_2 \tag{16}$$

The solutions of the corresponding algebraic equation include two types: the trivial solution ($a_1 = 0$ and $a_2 = 0$), and the non-trivial solution or coupled-mode solution ($a_1 \neq 0$ and $a_2 \neq 0$). Eliminating ψ_1 and ψ_2, we conclude that the steady-state response of the first mode is the root of the following frequency response equation. Due to the limitation of space, the explicit analytical expressions of a_1 and a_2 are not recorded here. Ultimately, the first approximate solutions can be written as

$$\tilde{q}_1 = a_1 \cos\left(\omega t/4 - (2\psi_1 + \psi_2)/4\right) + 2B_1 \cos\left(\omega t\right) + O\left(\varepsilon^2\right)$$
$$\tilde{q}_2 = a_2 \cos\left(\omega t/2 - \psi_2/2\right) + 2B_2 \cos\left(\omega t\right) + O\left(\varepsilon^2\right) \tag{17}$$
$$\tilde{q}_i = 0 \quad (i = 3, 4, \cdots, n_2 + n_3)$$

2.3. The Case of ω Being Close to $\omega_2 + \omega_1$

When ω is close to $\omega_2 + \omega_1$, the term $\bar{A}_j B_k \exp\left(i\left(\omega - \omega_j\right)T_0\right)(j = 2,\ k = 1$ or $2)$ contributes to the secular terms of the first mode, and in the same time, the term $\bar{A}_j B_k \exp\left(i\left(\omega - \omega_j\right)T_0\right)(j = 1,$ $k = 1$ or $2)$ contributes to the secular terms of the second mode. This resonance is often defined as the combination resonance of summed type. The external detuning parameter σ_2 is introduced as $\omega = \omega_2 + \omega_1 + \varepsilon\sigma_2$. After the mathematical manipulations similar to those in subsection 2.1, we can obtain the polar form of modulation equations.

$$\frac{da_1}{dT_1} = \left(\Gamma_{12}^R \cos\psi_1 - \Gamma_{12}^I \sin\psi_1\right)\frac{a_1 a_2}{2} + \left(\Gamma_{16}^R \cos\psi_2 - \Gamma_{16}^I \sin\psi_2\right) a_2 + \Gamma_{11}^R a_1$$

$$\frac{da_2}{dT_1} = \left(\Gamma_{22}^R \cos\psi_1 + \Gamma_{22}^I \sin\psi_1\right)\frac{a_1^2}{2} + \left(\Gamma_{26}^R \cos\psi_2 - \Gamma_{26}^I \sin\psi_2\right) a_1 + \Gamma_{21}^R a_2$$

$$\frac{d\psi_1}{dT_1} = \sigma_1 + \Gamma_{21}^I - 2\Gamma_{11}^I - \left(\Gamma_{12}^R \sin\psi_1 + \Gamma_{12}^I \cos\psi_1\right) a_2 + \left(\Gamma_{26}^R \sin\psi_2 + \Gamma_{26}^I \cos\psi_2\right)\frac{a_1}{a_2}$$
$$\qquad - \left(\Gamma_{16}^R \sin\psi_2 + \Gamma_{16}^I \cos\psi_2\right)\frac{2a_2}{a_1} - \left(\Gamma_{22}^R \sin\psi_1 - \Gamma_{22}^I \cos\psi_1\right)\frac{a_1^2}{2a_2}$$

$$\frac{d\psi_2}{dT_1} = \sigma_2 - \Gamma_{21}^I - \left(\Gamma_{12}^R \sin\psi_1 + \Gamma_{12}^I \cos\psi_1\right)\frac{a_2}{2} - \Gamma_{11}^I - \left(\Gamma_{16}^R \sin\psi_2 + \Gamma_{16}^I \cos\psi_2\right)\frac{a_2}{a_1}$$
$$\qquad + \left(\Gamma_{22}^R \sin\psi_1 - \Gamma_{22}^I \cos\psi_1\right)\frac{a_1^2}{2a_2} - \left(\Gamma_{26}^R \sin\psi_2 + \Gamma_{26}^I \cos\psi_2\right)\frac{a_1}{a_2} \tag{18}$$

where

$$\psi_1 = \sigma_1 T_1 - 2\zeta_1 + \zeta_2,\ \psi_2 = \sigma_2 T_1 - \zeta_1 - \zeta_2,\ \Gamma_{16} = \frac{\sum_{k=1}^{n_2+n_3}(\eta_{12k} + \eta_{1k2})B_k}{2i\omega_1},\ \Gamma_{26} = \frac{\sum_{k=1}^{n_2+n_3}(\eta_{21k} + \eta_{2k1})B_k}{2i\omega_2} \tag{19}$$

The solutions of the corresponding algebraic equation include two types the same as the previous subsection. Ultimately, the first approximate solutions can be written as

$$\tilde{q}_1 = a_1 \cos\left(\frac{\omega t}{3} - \frac{\psi_1 + \psi_2}{3}\right) + 2B_1 \cos(\omega t) + O(\varepsilon^2)$$

$$\tilde{q}_2 = a_2 \cos\left(\frac{2\omega t}{3} + \frac{\psi_1 - 2\psi_2}{3}\right) + 2B_2 \cos(\omega t) + O(\varepsilon^2) \tag{20}$$

$$\tilde{q}_i = 0 \quad (i = 3, 4, \ldots, n_2 + n_3)$$

2.4. The Case of ω Being Close to ω_2–ω_1

When ω is close to ω_2–ω_1, the term $A_j B_k \exp(\mathrm{i}(\omega_j + \omega)T_0)$ ($j = 1$, $k = 1$ or 2) contributes to the secular terms of the second mode. This resonance is often defined as the combination resonance of difference type. The external detuning parameter σ_2 is introduced as $\omega = \omega_2 - -\omega_1 + \varepsilon\sigma_2$. After the mathematical manipulations similar to those in subsection 2.1, we can obtain the polar form of modulation equations.

$$\frac{\mathrm{d}a_1}{\mathrm{d}T_1} = \Gamma_{11}^R a_1 + \left(\Gamma_{12}^R \cos\psi_1 - \Gamma_{12}^I \sin\psi_1\right)\frac{a_1 a_2}{2} + \left(\Gamma_{17}^R \cos\psi_2 - \Gamma_{17}^I \sin\psi_2\right)a_2$$

$$+ 2\left(\Gamma_{18}^R \cos(\psi_1 - \psi_2) - \Gamma_{18}^I \sin(\psi_1 - \psi_2)\right)$$

$$\frac{\mathrm{d}a_2}{\mathrm{d}T_1} = \Gamma_{21}^R a_2 + \left(\Gamma_{22}^R \cos\psi_1 + \Gamma_{22}^I \sin\psi_1\right)\frac{a_1^2}{2} + \left(\Gamma_{27}^R \cos\psi_2 + \Gamma_{27}^I \sin\psi_2\right)a_1$$

$$\frac{\mathrm{d}\psi_1}{\mathrm{d}T_1} = \sigma_1 + \Gamma_{21}^I - 2\Gamma_{11}^I - \left(\Gamma_{12}^R \sin\psi_1 + \Gamma_{12}^I \cos\psi_1\right)a_2 - \left(\Gamma_{17}^R \sin\psi_2 + \Gamma_{17}^I \cos\psi_2\right)\frac{2a_2}{a_1} - \left(\Gamma_{27}^R \sin\psi_2\right.$$

$$\left. - \Gamma_{27}^I \cos\psi_2\right)\frac{a_1}{a_2} - \left(\Gamma_{22}^R \sin\psi_1 - \Gamma_{22}^I \cos\psi_1\right)\frac{a_1^2}{2a_2} - \left(\Gamma_{18}^R \sin(\psi_1 - \psi_2) + \Gamma_{18}^I \cos(\psi_1 - \psi_2)\right)\frac{4}{a_1}$$

$$\frac{\mathrm{d}\psi_2}{\mathrm{d}T_1} = \Gamma_{21}^I - \Gamma_{11}^I - \sigma_2 - \left(\Gamma_{12}^R \sin\psi_1 + \Gamma_{12}^I \cos\psi_1\right)\frac{a_2}{2} - \left(\Gamma_{18}^R \sin(\psi_1 - \psi_2) + \Gamma_{18}^I \cos(\psi_1 - \psi_2)\right)\frac{2}{a_1}$$

$$- \left(\Gamma_{22}^R \sin\psi_1 - \Gamma_{22}^I \cos\psi_1\right)\frac{a_1^2}{2a_2} - \left(\Gamma_{27}^R \sin\psi_2 - \Gamma_{27}^I \cos\psi_2\right)\frac{a_1}{a_2} - \left(\Gamma_{17}^R \sin\psi_2 + \Gamma_{17}^I \cos\psi_2\right)\frac{a_2}{a_1} \tag{21}$$

where

$$\psi_1 = \sigma_1 T_1 - 2\zeta_1 + \zeta_2, \psi_2 = -\sigma_2 T_1 - \zeta_1 + \zeta_2, \Gamma_{17} = \sum_{k=1}^{n_2+n_3}(\eta_{12k} + \eta_{1k2})B_k/2\mathrm{i}\omega_1$$

$$\Gamma_{18} = \omega c_d B_1/2\omega_1, \Gamma_{27} = \sum_{k=1}^{n_2+n_3}(\eta_{21k} + \eta_{2k1})B_k/2\mathrm{i}\omega_2 \tag{22}$$

In the present case, it is hard to derive the analytical expressions of the coupled-mode solution due to the same reason as the subharmonic resonance of the first mode. The numerical approximate solution and the corresponding stability of the solutions can be determined following subsection 2.1. Ultimately, the first approximate solutions can be written as

$$\tilde{q}_1 = a_1 \cos(\omega t - (\psi_1 - \psi_2)) + 2B_1 \cos(\omega t) + O(\varepsilon^2)$$

$$\tilde{q}_2 = a_2 \cos(2\omega t - (\psi_1 - 2\psi_2)) + 2B_2 \cos(\omega t) + O(\varepsilon^2) \tag{23}$$

$$\tilde{q}_i = 0 \quad (i = 3, 4, \cdots, n_2 + n_3)$$

3. Validation and Perturbation Curves

In this section, the validation of free vibration component (a_1 and a_2) is conducted through the 4th-order Runge-Kutta method [31] and the frequency response and the force response curves are presented for the aforementioned four resonance cases. The equation of motion is integrated numerically. Only the past-transient motion is picked up to verify the analytical results. In the present study, parameters are chosen following the previous paper [20], namely $n_2 = n_3 = 10$, $\Psi = 10°$, $\Theta = 30°$, $\kappa = 0.25$, $\delta = 0$, $g_y = 0$, $g_z = 0.032$, $\eta = 200$, $c_d = 0.1$, and $\varepsilon = 0.01$. For the complete 2:1 internal resonance ($\sigma_1 =$

0) of this rotating blade, the critical rotating speed is $\gamma_{\text{in}} = 6.5798$, and the corresponding first two natural frequencies are $\omega_1 = 4.4873$ and $\omega_2 = 8.9746$.

3.1. Subharmonic Resonance of the First Mode

From the first equation in Eq. (14), it is found that the free vibration component of the first mode response, namely the frequency component of $\omega/2$, is separated from the forced vibration component, namely the frequency component of ω. So the free vibration component amplitude a_1 can be determined directly from the fast Fourier transform (FFT) of the blade response. However, the situation is more complicated for the second mode response. The free vibration component and the forced vibration component share the same frequency ω. To verify the free vibration component amplitude a_2, the second equation of Eq. (14) is cast into

$$\tilde{q}_2 = Q_2 \cos\left(\omega t + \nu_2\right) + O\left(\varepsilon^2\right) \tag{24}$$

in which Q_2 and ν_2 stand for the magnitude and phase angle of the frequency component of ω, respectively, and hold the following relationships.

$$Q_2 = \sqrt{a_2^2 + 4B_2^2 + 4a_2 B_2 \cos\left(\psi_1 - \psi_2\right)}$$
$$\cos\nu_2 = \frac{a_2 \cos\left(\psi_1 - \psi_2\right) + 2B_2}{Q_2} \tag{25}$$

Eliminating ψ_1 and ψ_2 yields

$$a_2 = \sqrt{4B_2^2 + Q_2^2 - 4B_2 Q_2 \cos\nu_2} \tag{26}$$

In the equation above, B_2 is calculated from Eq. (7), Q_2 and ν_2 are determined from the FFT. Eq. (26) can be used to verify the free vibration component amplitude a_2. The comparison between the frequency responses obtained from theoretical analysis and numerical integrations is displayed in Fig. 2. The solid and dotted lines denote the stable and unstable solutions calculated by the method of multiple scales, respectively. The hollow circles and asterisks denote the results obtained from the numerical integrations of the original system and the modulation equations, respectively. As seen in Fig. 2, the steady solutions seem to be attracted to the single-mode solution near the jumping [32]. The theoretical results are well consistent with the numerical integrations.

The influences of system parameters on frequency response curves are illustrated in Fig. 3. The response curves tend to bend more to both sides and the peak responses are enlarged with the increase of thermal gradient. Actually, the thermal gradient presents quadratic nonlinearities of the system in some sense. The response curves will tilt to the right with the increase of rotating speed across the internal critical rotating speed γ_{in}. It has been reported in the literature [17, 19] that the variation in rotating speed will result in the variation in nonlinear hardening/softening behavior of the rotating
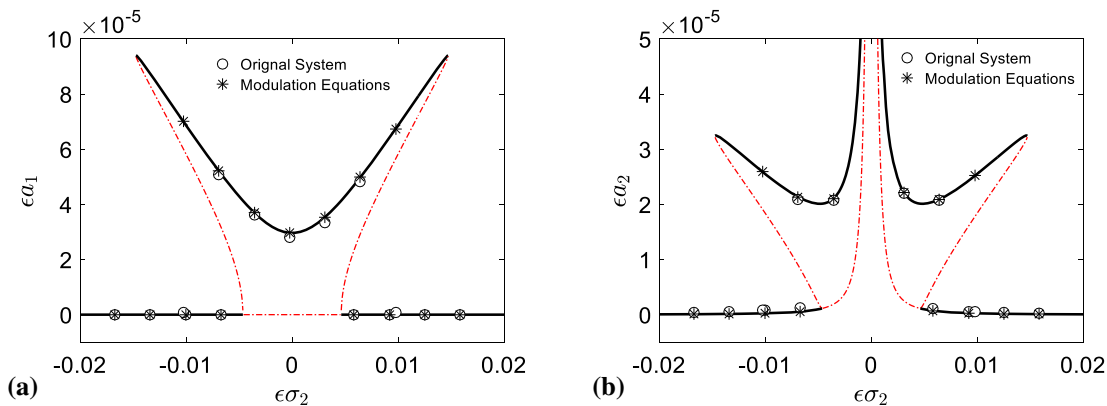

Fig. 2. The comparison between the frequency responses obtained from theoretical analysis and numerical integrations in the case of subharmonic resonance of the first mode ($P_{\text{gas}} = 10^{-4}$): **a** the first mode; **b** the second mode
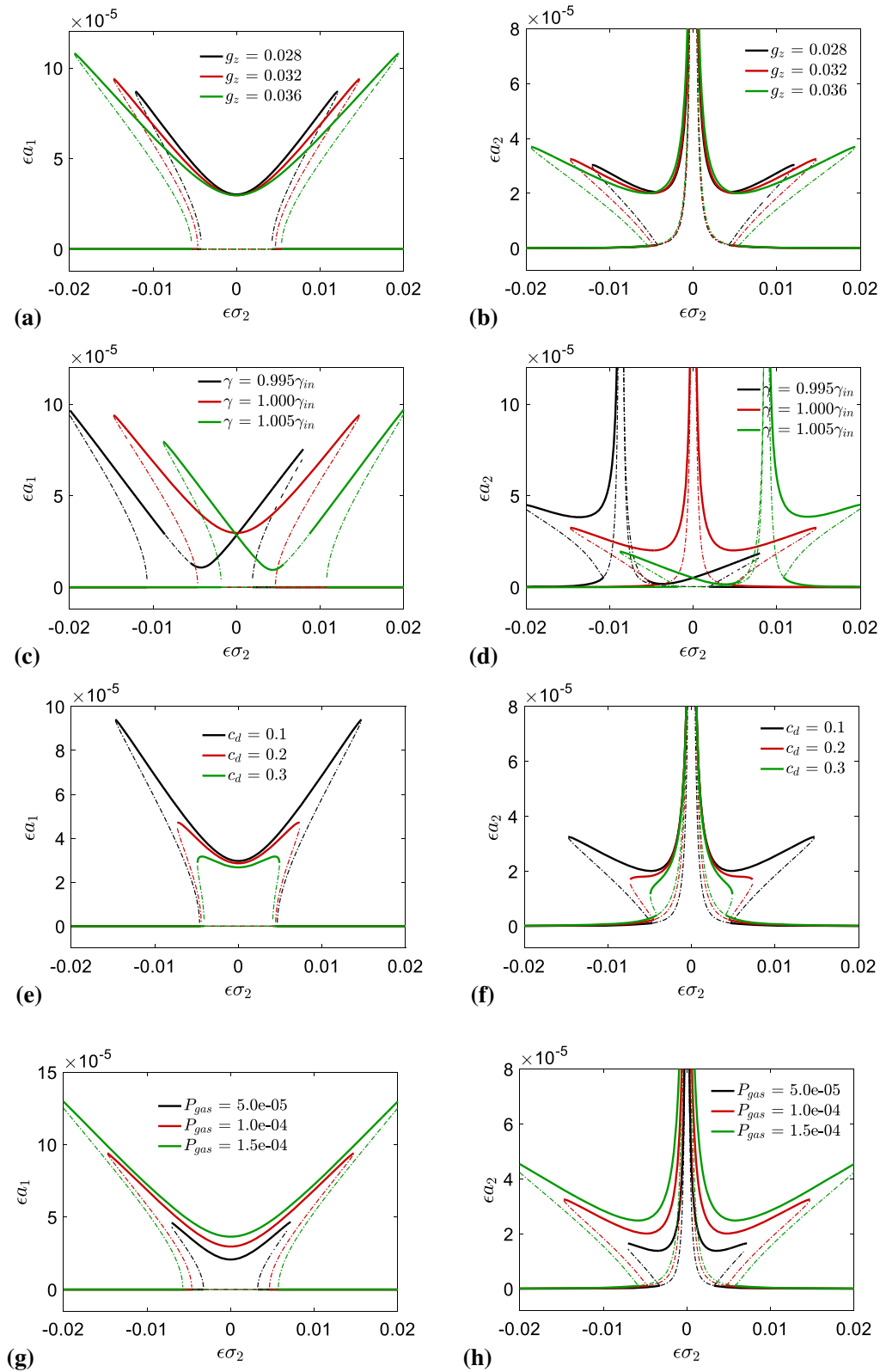
Fig. 3. Parameter study of frequency response curves in the case of subharmonic resonance of the first mode: **a**, **b** the influence of thermal gradient; **c**, **d** the influence of rotating speed; **e**, **f** the influence of damping coefficient; **g**, **h** the influence of gas pressure
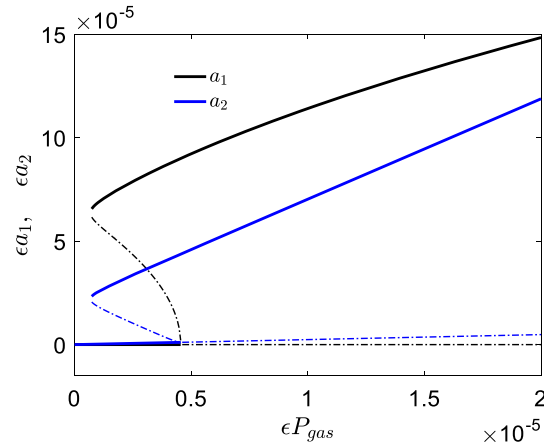
Fig. 4. The subharmonic force response curves of the first and the second modes in the case of subharmonic resonance of the first mode ($\sigma_1 = 0$, $\sigma_2 = 1$)
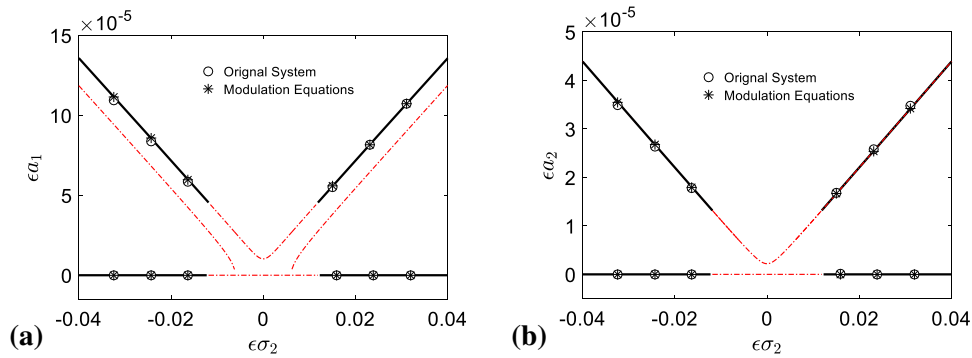

Fig. 5. The comparison between the frequency responses obtained from theoretical analysis and numerical integrations in the case of subharmonic resonance of the second mode ($P_{\mathrm{gas}} = 0.5$): **a** the first mode; **b** the second mode

blade. The jumping phenomena are limited by the damping. With the increase of damping coefficient, the peak responses are reduced and the multi-valued ranges are narrowed. The response curves tend to be flattened for large damping coefficient. However, as expected, the gas pressure seems to have an opposite influence on the response curves. The jumping phenomena become dramatic with the increase of the gas pressure. Both the peak response and the multi-valued ranges are enlarged by the gas pressure. The variation trends of the frequency response curve with parameters in other resonance cases are similar to the present one. Hence, the related results are not displayed herein.

The force response curves of the first and the second modes are plotted together in Fig. 4. A hysteresis phenomenon occurs. The single-mode solution turns unstable when the gas pressure increases beyond the first limit point. Compared with the coupled-mode solution, the single-mode solution of the second mode is quite small and negligible.

3.2. Subharmonic Resonance of the Second Mode

For the first two modes of response, the free vibration components are separated from the forced vibration components in the case of subharmonic resonance of the second mode. So the free vibration component amplitudes a_1 and a_2 can be determined directly from FFT of the blade response. The comparisons between the frequency responses obtained from the theoretical analysis and the numerical integrations are displayed in Fig. 5. The theoretical results agree well with the numerical simulation. The non-trivial solutions of the first two modes are both v-shaped. Both the trivial and non-trivial solutions are unstable near the totally external resonance. In order to present the full view of the
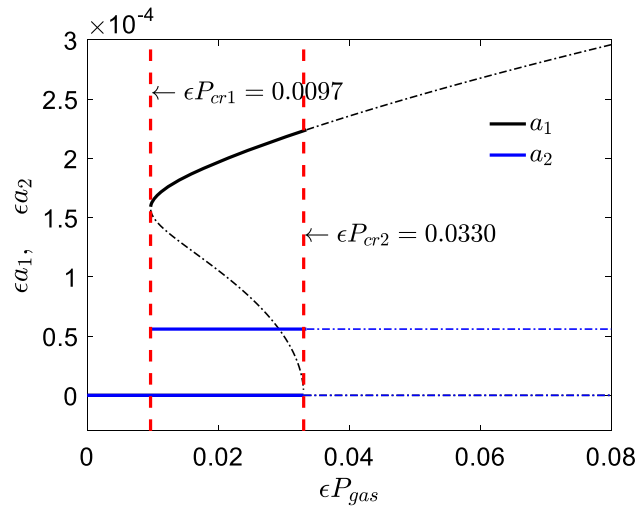
Fig. 6. The subharmonic force response curves of the first and the second modes in the case of subharmonic resonance of the second mode ($\sigma_1 = 0$, $\sigma_2 = 5$)
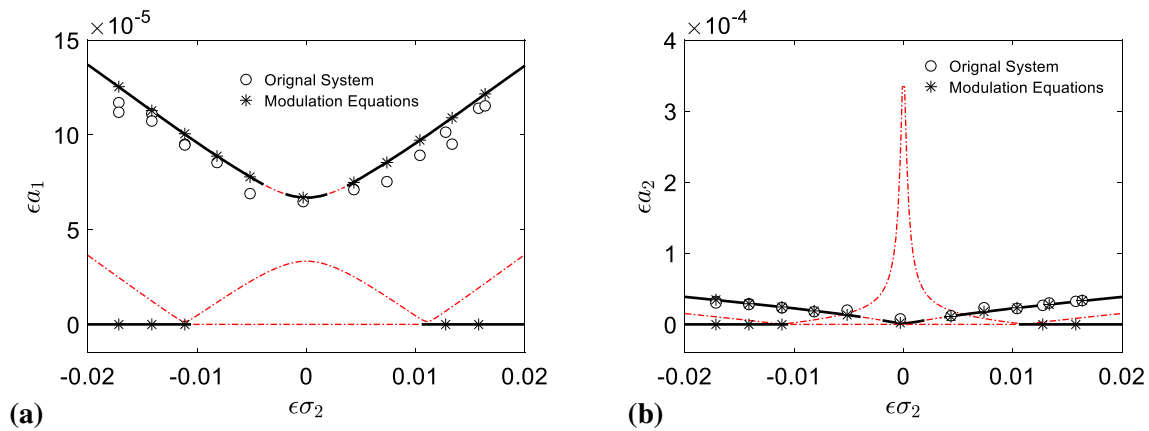

Fig. 7. The comparison between the frequency responses obtained from theoretical analysis and numerical integrations in the case of combination resonance of summed type ($P_{\text{gas}} = 1$): **a** the first mode; **b** the second mode

dynamic behavior, the gas pressure is set as a quite large value, $P_{\text{gas}} = 0.5$. To a certain extent, this indicates that the subharmonic resonance of the second mode is hard to excite.

The force response curves are plotted in Fig. 6. A saturation phenomenon [33] can be observed. There exist two critical values of gas pressure, P_{cr1} and P_{cr2}, between which there exist two non-trivial solutions for a_1 (the lager one is stable) and the second-mode response keeps constant. It seems that the external energy is only imported into the first mode.

3.3. Combination Resonance of Summed Type

The free vibration components are separated from the forced vibration components in the case of combination resonance of summed type. So the free vibration component amplitudes a_1 and a_2 can be determined directly from FFT of the blade response. The comparison between the frequency responses obtained from theoretical analysis and numerical integrations is displayed in Fig. 7. It can be found that the non-trivial equilibrium points have strong attraction and several trivial equilibrium points are attracted to the non-trivial ones. The gas pressure here is quite strong as the previous case. The trivial solution is unstable near the total external resonance ($\sigma_2 = 0$). There exist certain ranges, in which both the non-trivial and the trivial solutions are unstable and the response will be quasi-periodic motion or chaos.
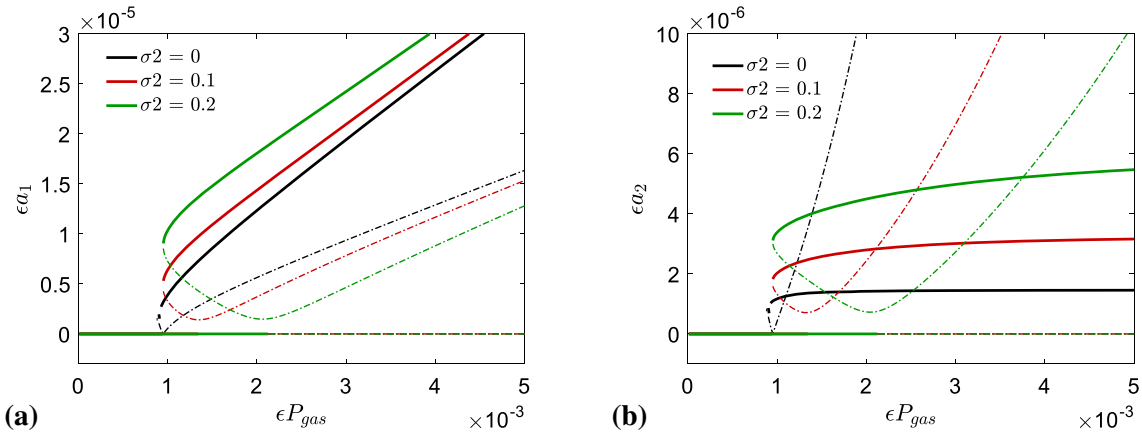
Fig. 8. The force response curves of the first and the second modes in the case of combination resonance of summed type ($\sigma_1 = 0$): **a** the first mode; **b** the second mode
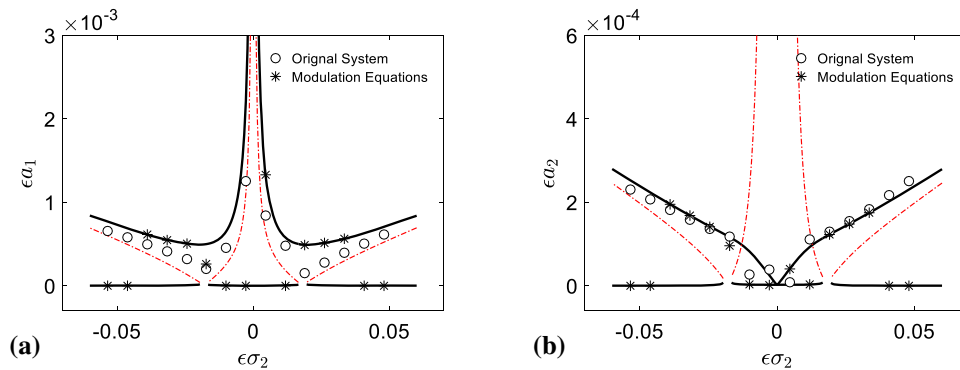

Fig. 9. The comparison between the frequency responses obtained from theoretical analysis and numerical integrations in the case of combination resonance of difference type (Pgas $= 0.01$): **a** the first mode; **b** the second mode

Figure 8 shows the force response curves for certain values of σ_2. In the flapwise primary resonance under low gas pressure [20], the second-mode response is independent of gas pressure after saturated. In the present case, after a certain value, the second-mode response changes rather slightly with gas pressure when compared with the first-mode response. The vast majority of the external energy carried in the gas pressure pours into the first mode. A quasi-saturation phenomenon can be found. The prefix "quasi-" is used to emphasize the difference between the present phenomenon and the saturation phenomenon [20]. The quasi-saturation phenomenon can only occur at high gas pressure. The limit value of the second-mode response can be reduced by decreasing the external detuning parameter σ_2. In the design stage of such structure, engineers may utilize the quasi-saturation phenomenon to control the quantity and direction of energy transfer from the gas excitation to the vibration of the blade.

3.4. Combination Resonance of Difference Type

From Eq. (23), it is found that for the second-mode response, the free vibration component is separated from the forced vibration components in the case of combination resonance of difference type. While the free vibration of the first mode share the same frequency with the forced vibration component. Hence, the free vibration component amplitude a_2 can be determined directly from FFT of the blade response, and a_1 can be verified following subsection 3.1. The comparison between the frequency responses obtained from theoretical analysis and numerical integrations is displayed in Fig. 9. There exist three solutions in most situations. The minimum changes slightly with the external detuning parameter and approximates to zero solution. Both the maximum and the minimum are stable. The
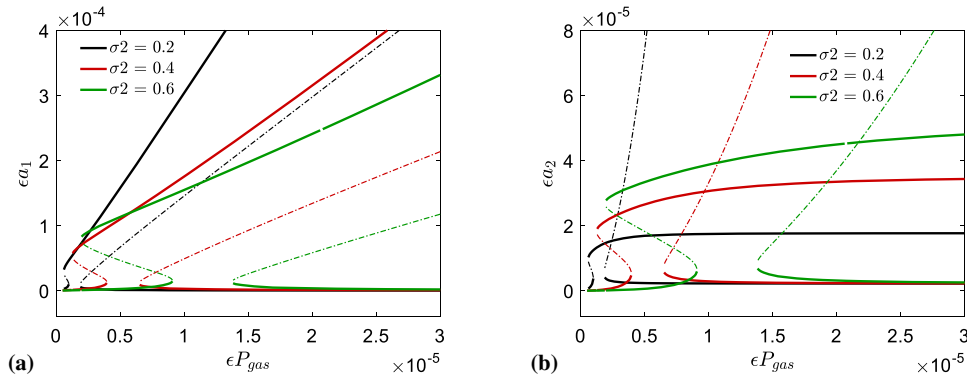
Fig. 10. The force response curves of the first and the second modes in the case of combination resonance of difference type ($\sigma_1 = 0$): **a** the first mode; **b** the second mode

response depends on the initial conditions. The theoretical analysis is in agreement with the numerical integrations.

The force response curves for several different values of σ_2 are presented in Fig. 10. A quasi-saturation phenomenon can be found, which is similar to subsection 3.3.

4. Conclusion

In this paper, we consider four resonance cases of a rotating blade subjected to harmonic gas pressure in the presence of 2:1 internal resonance. The method of multiple scales is applied to obtain the steady-state response. The theoretical results are supported by the numerical simulation. For the case of the subharmonic resonance of the first mode, a hysteresis phenomenon occurs and the single-mode solution of the second mode is negligible when compared with the coupled-mode solution. The quasi-saturation phenomenon of the rotating blade only occurs with high gas pressure. The limit value of the second mode response can be reduced by decreasing the external detuning parameter in the two cases of combination resonance. The dynamic behavior observed is expected to be useful for the design of such structure.

References

[1] Leissa AW, Lee JK, Wang AJ. Vibrations of twisted rotating blades. J Vib Acoust. 1984;106(2):251–7.

[2] Kane TR, Ryan RR, Banerjee AK. Dynamics of a cantilever beam attached to a moving base. J Guid Control Dynam. 1987;10(2):139–51. https://doi.org/10.2514/3.20195.

[3] Yoo HH, Shin SH. Vibration analysis of rotating cantilever beams. J Sound Vib. 1998;212(5):807–28. https://doi.org/10.1006/jsvi.1997.1469.

[4] Banerjee JR. Free vibration of centrifugally stiffened uniform and tapered beams using the dynamic stiffness method. J Sound Vib. 2000;233(5):857–75. https://doi.org/10.1006/jsvi.1999.2855.

[5] Chiu YJ, Yang CH. The coupled vibration in a rotating multi-disk rotor system with grouped blades. J Mech Sci Technol. 2014;28(5):1653–62. https://doi.org/10.1007/s12206-014-0310-4.

[6] Li L, Zhang XL, Li YH. Analysis of coupled vibration characteristics of wind turbine blade based on green's functions. Acta Mech Solida Sin. 2016;29(6):620–30.

[7] Qin Y, Li YH. Influences of hygrothermal environment and installation mode on vibration characteristics of a rotating laminated composite beam. Mech Syst Signal Process. 2017;91:23–40. https://doi.org/10.1016/j.ymssp.2016.12.041.

[8] Liang F, Li Z, Yang XD, Zhang W, Yang TZ. Coupled bending-bending-axial-torsional vibrations of rotating blades. Acta Mech Solida Sin. 2019;32(3):326–38. https://doi.org/10.1007/s10338-019-00075-w.

[9] Niu Y, Zhang W, Guo XY. Free vibration of rotating pretwisted functionally graded composite cylindrical panel reinforced with graphene platelets. Eur J Mech Solid. 2019;77:103798. https://doi.org/10.1016/j.euromechso1.2019.103798.

[10] Zhang W, Niu Y, Behdinan K. Vibration characteristics of rotating pretwisted composite tapered blade with graphene coating layers. Aerosp Sci Technol. 2020;. https://doi.org/10.1016/j.ast.2019.105644.

[11] Guo XY, Yang XD, Wang SW. Dynamic characteristics of a rotating tapered cantilevered timoshenko beam with preset and pre-twist angles. Int J Struct Stab Dyn. 2019;. https://doi.org/10.1142/S0219455419500433.

[12] Xie JS, Zi YY, Zhang MQ, Luo QY. A novel vibration modeling method for a rotating blade with breathing cracks. Sci China Technol Sci. 2019;62(2):333–48. https://doi.org/10.1007/s11431-018-9286-5.

[13] Moffatt S, Ning W, Li YS, Wells RG, Li H. Blade forced response prediction for industrial gas turbines. J Propul Power. 2005;21(4):707–14. https://doi.org/10.2514/1.6126.

[14] Ding H, Huang L-L, Dowell E, Chen L-Q. Stress distribution and fatigue life of nonlinear vibration of an axially moving beam. Sci China Technol Sci. 2019;. https://doi.org/10.1007/s11431-017-9283-4.

[15] Li YH, Li L, Liu QK, Lv HW. Dynamic characteristics of lag vibration of a wind turbine blade. Acta Mech Solida Sin. 2013;26(6):592–602. https://doi.org/10.1016/S0894-9166(14)60004-5.

[16] Yao MH, Niu Y, Hao YX. Nonlinear dynamic responses of rotating pretwisted cylindrical shells. Nonlinear Dyn. 2019;95(1):151–74. https://doi.org/10.1007/s11071-018-4557-7.

[17] Thomas O, Senechal A, Deu JF. Hardening/softening behavior and reduced order modeling of nonlinear vibrations of rotating cantilever beams. Nonlinear Dyn. 2016;86(2):1293–318. https://doi.org/10.1007/s11071-016-2965-0.

[18] Wang D, Chen YS, Hao ZF, Cao QJ. Bifurcation analysis for vibrations of a turbine blade excited by air flows. Sci China Technol Sci. 2016;59(8):1217–31. https://doi.org/10.1007/s11431-016-6064-8.

[19] Zhang B, Li YM. Nonlinear vibration of rotating pre-deformed blade with thermal gradient. Nonlinear Dyn. 2016;86(1):459–78. https://doi.org/10.1007/s11071-016-2900-4.

[20] Zhang B, Zhang Y-L, Yang X-D, Chen L-Q. Saturation and stability in internal resonance of a rotating blade under thermal gradient. J Sound Vib. 2019;440(3):34–50. https://doi.org/10.1016/j.jsv.2018.10.012.

[21] Cao DX, Liu BY, Yao MH, Zhang W. Free vibration analysis of a pre-twisted sandwich blade with thermal barrier coatings layers. Sci China Technol Sci. 2017;60(11):1747–61. https://doi.org/10.1007/s11431-016-9011-5.

[22] Inoue T, Ishida Y, Kiyohara T. Nonlinear vibration analysis of the wind turbine blade (occurrence of the superharmonic resonance in the out of plane vibration of the elastic blade). ASME J Vib Acoust. 2012;. https://doi.org/10.1115/1.4005829.

[23] Zhang B, Ding H, Chen LQ. Super-harmonic resonances of a rotating pre-deformed blade subjected to gas pressure. Nonlinear Dyn. 2019;98(4):2531–49. https://doi.org/10.1007/s11071-019-05367-x.

[24] Shahgholi M, Khadem SE. Internal, combinational and sub-harmonic resonances of a nonlinear asymmetrical rotating shaft. Nonlinear Dyn. 2015;79(1):173–84. https://doi.org/10.1007/s11071-014-1654-0.

[25] Mook DT, Plaut RH, HaQuang N. The influence of an internal resonance on non-linear structural vibrations under subharmonic resonance conditions. J Sound Vib. 1985;102(4):473–92. https://doi.org/10.1016/S0022-460X(85)80108-5.

[26] Mook DT, HaQuang N, Plaut RH. The influence of an internal resonance on non-linear structural vibrations under combination resonance conditions. J Sound Vib. 1986;104(2):229–41. https://doi.org/10.1016/0022-460X(86)90265-8.

[27] Elnaggar AM, El-Basyouny AF. Harmonic, subharmonic, superharmonic, simultaneous sub/super harmonic and combination resonances of self-excited two coupled second order systems to multi-frequency excitation. Acta Mech Sin. 1993;9(1):61–71. https://doi.org/10.1007/bf02489163.

[28] Ma H, Xie FT, Nai HQ, Wen BC. Vibration characteristics analysis of rotating shrouded blades with impacts. J Sound Vib. 2016;378:92–108. https://doi.org/10.1016/j.jsv.2016.05.038.

[29] Ma H, Yin FL, Guo YZ, Tai XY, Wen BC. A review on dynamic characteristics of blade-casing rubbing. Nonlinear Dyn. 2016;84(2):437–72. https://doi.org/10.1007/s11071-015-2535-x.

[30] Tang YQ, Chen LQ, Yang XD. Nonlinear vibrations of axially moving timoshenko beams under weak and strong external excitations. J Sound Vib. 2009;320(4–5):1078–99. https://doi.org/10.1016/j.jsv.2008.08.024.

[31] Li X, Zhang YW, Ding H, Chen LQ. Integration of a nonlinear energy sink and a piezoelectric energy harvester. Appl Math Mech-Engl. 2017;38(7):1019–30. https://doi.org/10.1007/s10483-017-2220-6.

[32] Lu ZQ, Hu GS, Ding H, Chen LQ. Jump-based estimation for nonlinear stiffness and damping parameters. J Vib Control. 2019;25(2):325–35. https://doi.org/10.1177/1077546318777414.

[33] Ding H, Huang LL, Mao XY, Chen LQ. Primary resonance of traveling viscoelastic beam under internal resonance. Appl Math Mech-Engl. 2017;38(1):1–14. https://doi.org/10.1007/s10483-016-2152-6.